Photonic crystal composites-based wide-band optical collimator

Jinjie Shi,[1] Bala Krishna Juluri,[1] Sz-Chin Steven Lin,[1] Mengqian Lu,[1] Tieyu Gao,[2,a)] and Tony Jun Huang[1,a)]
[1]*Department of Engineering Science and Mechanics, The Pennsylvania State University, University Park, Pennsylvania 16802, USA*
[2]*School of Energy and Power Engineering, Xi'an Jiaotong University, Xi'an, Shaanxi 710049, China*

(Received 19 May 2010; accepted 30 June 2010; published online 23 August 2010)

Photonic crystal (PC) composites are sequenced series of PCs that feature the same periods but different filling fractions. By properly tuning the filling fractions of the individual PCs and merging the working band of each PC into a continuous frequency range, wide-band self-collimation of optical signals can be realized. The band diagrams and the equal-frequency contours of the PC structures were calculated through the plane wave expansion method and the finite-difference time-domain method was employed to simulate the propagation of electromagnetic waves through the PC structures. Our results show that while a single PC can only collimate optical waves over a narrow frequency range, a PC composite exhibits a much wider collimation band. Such a wide-band optical collimation lens can be useful in applications that demand directional optical energy flow over a long distance, such as optical imaging and biosensing. © *2010 American Institute of Physics*. [doi:10.1063/1.3468242]

I. INTRODUCTION

Periodically distributed structures of dielectric materials called photonic crystals (PCs) have attracted much interest from both academia and industry in the past two decades because PCs grant the ability to manipulate electromagnetic waves through relatively simple configurations.[1–3] Researchers have observed many interesting phenomena (e.g., band gaps,[4] negative refraction,[5–7] and photon tunneling[8]) in PCs and have developed manifold applications such as fibers, waveguides, micro/nanocavity lasers, beam splitters, and biological/chemical sensors. Flat slabs of PCs have recently been engineered to collimate electromagnetic waves at designated frequencies where the curvatures of the equal-frequency contours (EFCs) in k-space are nearly zero.[9–16] Such diffractionless propagation in a PC is described as *self-collimating* or *self-guiding*. PC-based collimation lenses can be made much smaller than traditional collimation lenses (with curved surfaces) and production of such lenses by micromachining techniques is straightforward and inexpensive. These advantages enable the mass-production of collimation devices at the microscale, where traditional convex and concave lenses[17] are extremely difficult to fabricate.

Despite these advantages, single PC-based collimation lenses only work within a narrow frequency band where the EFCs are flat, since the EFC curvature of a PC changes dramatically with frequency. Periodic composite structures have been previously designed to steer wave beams.[16,18–25] In a previous study we have found that the self-collimation frequency band can be enlarged with phononic crystal composites, which are sequenced series of phononic crystals that have the same periods with different filling fractions.[16] In comparison with existing, single phononic crystal-based collimation lenses, phononic crystal composite-based collimation lenses exhibit larger spectral collimation ranges. By analogy, we expect PC-composites, the photonic counterparts of phononic crystal-composites, can expand the collimation ranges of PCs for electromagnetic waves.

The band diagrams and EFCs of two-dimensional (2D) PCs were calculated based on the plane wave expansion (PWE) method to predict the self-collimation direction and the working bands of self-collimation of PC structures (single PCs as well as PC composites). A finite-difference time-domain (FDTD) method was employed to simulate the electromagnetic wave propagation phenomena of PC structures and to demonstrate the wide-band self-collimation of PC composites. The self-collimation of single PCs is introduced in Sec. II. The working mechanism of wide-band self-collimation of PC composites is discussed in Sec. III. Finally, the simulated wave-propagation patterns that reveal the wide-band optical collimating properties of the PC composites are presented in Sec. IV.

II. SELF-COLLIMATION OF SINGLE PCS

A beam of electromagnetic wave is called *self-collimated* or *self-guided* if it does not spread when propagating in a PC.[10] The direction of energy propagation in a PC is given by the group velocity of the wave beam: $v_g = \nabla_k \omega(\boldsymbol{k})$ where ω is the angular frequency and $\boldsymbol{k}$ is the wave vector. This depicts that electromagnetic waves propagate along directions normal to EFCs, which demonstrate near-zero curvatures at certain frequencies in PC structures. At such frequencies, when incident waves (with varying wave vectors $\boldsymbol{k}$) end at the flat region of an EFC, they are all refracted normal to the flat contour. As a result, the energy fluxes are in the same direction, indicating self-collimation.

There are several methods to calculate the band diagrams and EFCs of PCs: the multiple scattering theory (MST) method,[26,27] the FDTD method,[28] the PWE

[a)]Electronic addresses: sunmoon@mail.xjtu.edu.cn and junhuang@psu.edu.

 © 2010 American Institute of Physics

Downloaded 14 Mar 2011 to 130.203.246.87. Redistribution subject to AIP license or copyright; see http://jap.aip.org/about/rights_and_permissions

method,[29–31] and the layer-multiple-scattering method.[32,33] We used the PWE method due to its strength in solving the vectorial eigenmodes of Maxwell's equations for periodic boundary conditions.[3] We have already employed the PWE method to demonstrate the wide-band collimation of acoustic waves through phononic crystals, acoustic analog of PCs.[16] Due to the spatial periodicity of a PC structure, the material properties (e.g., mass density and elastic stiffness tensor) can be expanded in Fourier series with respect to the reciprocal lattice vectors based on Bloch's theorem.[29–31] The accuracy of such calculations depends on the number of the terms used in the series expansion. In this work, 121×121 plane waves, corresponding to a mesh of 121 points in each of the reciprocal lattice directions, were used in the calculation of band diagrams to reach precise results.

Two single 2D PCs, which we used to investigate self-collimation phenomena, were solid/air PCs consisting 2D square arrays of rigid gallium nitride (GaN) cylinders immersed in air. The dielectric constants of GaN and air are 8.9 and 1.0, respectively. The lattice constant a of two single PCs was the same but the filling fraction ($\pi r^2/a^2$, where r is the radius of the cylinder) of the first PC (PC_1) was 0.2513 and that of the second PC (PC_2) was 0.1924. To simplify the calculation, we focused our investigation on the in-plane propagation of only the TM-polarization mode (where the electric field is parallel to the axes of the cylinders).

Figure 1 shows band diagrams for the first three TM-polarized bands of PC_1 and PC_2. The differences in filling fractions resulted in the slope change in dispersion curves, where a higher filling fraction resulted in a smaller slope. Both PCs demonstrated a complete band gap ranging from M_{11} to X_{12} for PC_1 and M_{21} to X_{22} for PC_2 with relative bandwidths (bandwidth divided by central frequency) of 29% and 31%, respectively. There was also a partial band gap in the ΓX orientation with the normalized frequency Ω (defined as $\omega a/2\pi c$, where c is the speed of light in air) extending from 0.2658 to 0.3164 (corresponding to points X_{11} and M_{11}) for PC_1, and from 0.2897 to 0.3405 (corresponding to points X_{21} and M_{21}) for PC_2. Figures 1(b) and 1(c) show the EFCs for the first band of PC_1 and PC_2, respectively. As the normalized frequency Ω was increased, the EFC curvatures of both PCs turned from convex to concave. In this transition process of the EFCs' curvatures from convex to concave, the flat regions on the EFCs, which were normal to the ΓM orientation, enlarged steadily with frequency and then reduced gradually after reaching their maxima ($\Omega=0.2864$ for PC_1 and $\Omega=0.2970$ for PC_2; bold solid curves). The boundaries of the longest flat regions were indicated by the solid arrows which point along the energy-propagating direction. These maxima indicate the frequencies at which the self-collimation angle, the region within which wave vectors (dashed arrows) undergo self-collimation along the ΓM orientation, was largest (shaded regions). By considering the conservation of the transverse momentum at the input boundary,[9] the construction lines (solid lines) were obtained by connecting the boundaries of the longest flat regions to the EFC of air (dotted curves) along the ΓM orientation. The dotted arrows indicate the wave vectors of largest incident angles that can be self-collimated by PCs in air. Within the collimation angles θ_{C1} and θ_{C2} (corresponding, respectively, to PC_1 and PC_2), all incident waves were self-collimated.

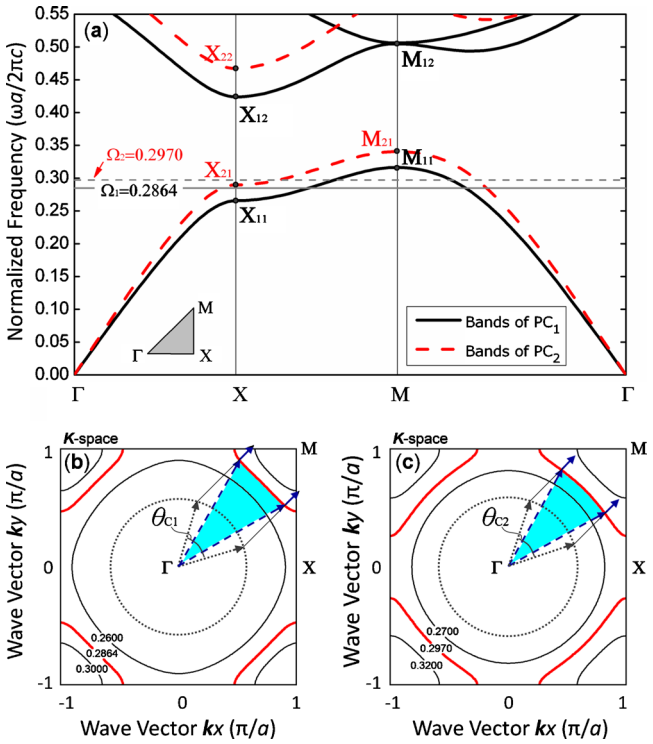

FIG. 1. (Color online) (a) First three TM polarized bands of PC_1 (solid) and PC_2 (dashed), composed of rigid GaN cylinders in air with filling fractions of 0.2513 and 0.1924, respectively. (b) and (c) are the first TM-polarized EFCs of PC_1 and PC_2, respectively. The bold solid curves indicate the EFCs of maximum self-collimation frequency and the dotted curves indicate the corresponding EFCs in air. The dashed and dotted arrows denote the wave vectors in PCs and air, respectively. The solid arrows indicate the boundaries of the flat band and the direction of the group velocity, and the shaded region shows the wave vectors that undergo self-collimation due to flat bands. The propagating waves within the collimation angle θ_C were collimated to the ΓM orientation.

III. WIDE-BAND SELF-COLLIMATION OF PC COMPOSITES

Although self-collimation can be achieved with a single PC structure as demonstrated in Fig. 1, such collimation system can only work over a narrow frequency range.[9–15] As the frequency deviates from the maximum self-collimation frequency ($\Omega=0.2864$ for PC_1 and $\Omega=0.2970$ for PC_2), the contour of the EFC changes into a circular geometry and only a small portion of the EFC depicts a near-zero curvature (Fig. 1). Such circular geometries permit only waves within a certain incident angle θ_C to be collimated, thereby limiting the use of single PC-based optical collimator. The collimation angle (θ_C)-frequency relations of PC_1 and PC_2 are shown in Fig. 2, where the collimation angle was determined as the maximum incident angle within which all refracted waves are less than $\pm 2.5°$ with respect to the ΓM orientation. At $\theta_C=25°$, the normalized frequency ranges of the collimation regions for PC_1 and PC_2 were calculated to be 0.282–0.291 (Δf_1) and 0.292–0.304 (Δf_2), respectively.

Figure 3(a) illustrates the propagation of electromagnetic waves that were emitted from a point source placed on the

Downloaded 14 Mar 2011 to 130.203.246.87. Redistribution subject to AIP license or copyright; see http://jap.aip.org/about/rights_and_permissions

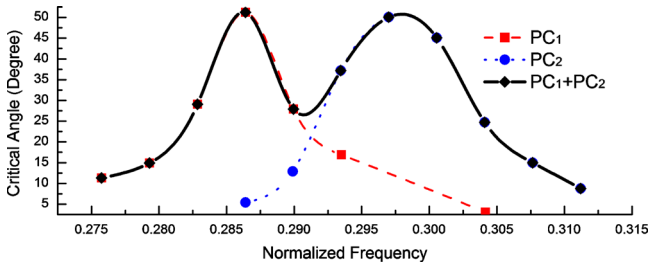

FIG. 2. (Color online) The dependence of collimation angles on normalized frequency for PC_1, PC_2, and PC_1+PC_2.

left side of a single PC at a frequency with concave EFC. The solid and dashed arrows indicate the wave propagation directions in air and PC, respectively. While incident waves within the collimation angle θ_C were self-collimated along the ΓM orientation by the PC, incident waves outside θ_C were negative refracted toward the center of the self-collimated beam. This deformed the wavefront after the waves passed through the PC, thereby limiting the use of single PC-based optical collimation lenses.

In order to overcome the limitations of single PC-based lenses, we designed a wide-band collimating lens from a series of PCs having the same periods but different filling fractions. Such a PC composite can self-collimate electromagnetic waves in a frequency band which is the summation of the narrow self-collimation bands of each PC that forms the PC composite.

To illustrate the mechanism, a 2D PC composite consisted of two 2D PCs (PC_1 and PC_2 in Sec. II) is shown in Fig. 3(b). The cylinders in PC_1 and PC_2 were oriented in a similar fashion, and the first columns of the subsequent PC (PC_2) were positioned exactly at the periodic frame of the previous PC (PC_1). A point source was placed on the left of the structure. For the emitted electromagnetic waves with different frequencies, two cases were involved: (1) when waves passed through the first PC (PC_1) at frequencies near the maximum self-collimation frequency of PC_1 ($\Omega_{m1}=0.2864$), the incident waves within the collimation angle θ_{C1} of PC_1 self-collimated along the ΓM orientation and remained unchanged (along ΓM orientation) as they propagated in PC_2. Since the collimation angle of PC_2 (θ_{C2}) was smaller than θ_{C1} in this frequency range, PC_1 dominated the EM collimation behavior and PC_2 retained the self-collimated beam. (2) When electromagnetic waves were emitted at frequencies near the maximum self-collimation frequency of PC_2 ($\Omega_{m2}=0.2970$, $\theta_{C2}>\theta_{C1}$ in this case), few of the waves (within collimation angle θ_{C1}) were guided by PC_1 along the ΓM orientation [blue dashed arrows in Fig. 3(b)]. The waves outside the collimation angle θ_{C1} were subject to negative refraction as they passed through PC_1 toward the center of the self-collimated beam, due to the concave-like EFC (red dashed arrows). Not self-collimated by PC_1, the incident waves with angles less than the collimation angle θ_{C2} of PC_2 ($\theta_{C2}>\theta_{C1}$) were subject to self-collimation upon propagating through PC_2 (red dash arrows). In this case, PC_2 was the major contributor to self-collimation, and the function of PC_1 was to confine the out-spreading energy to the center of the self-collimated beam. The PC composite thereby enlarged the self-collimation frequency bands by combining frequency bands of two single-PC structures. As shown in Fig. 2, for example, the PC composite significantly enlarges the collimation region by $\Delta f/\Delta f_1=267\%$ and $\Delta f/\Delta f_2=178\%$ at $\theta_C=25°$. Such a PC composite (PC_1+PC_2) may serve as the basis of an optical collimation lens that focuses waves of a wide frequency range; this idea can be extended to PC composites with more than two PCs with the compensation of higher transmission loss.

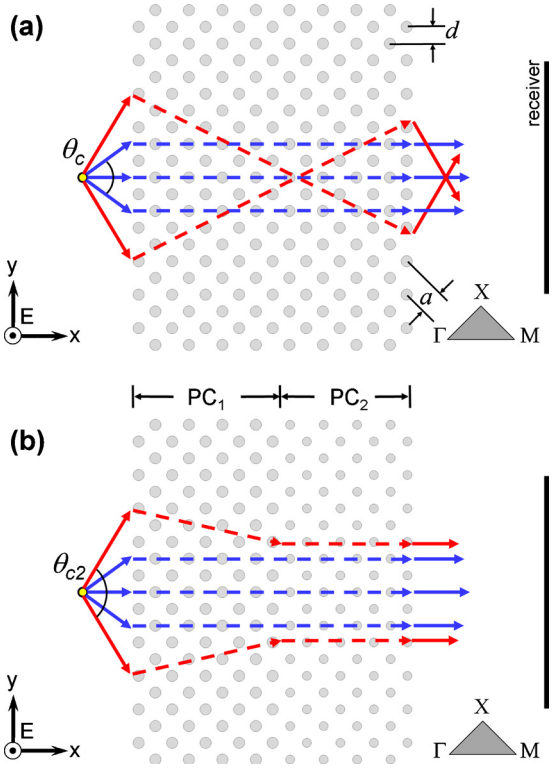

FIG. 3. (Color online) (a) Single PC structure (PC_1 or PC_2) that had homogenous periodicity and homogenous filling fractions. (b) A PC composite consisting of two PCs of the same periodicity but different filling fractions. A point source was placed on the left side of each PC structure. Arrows indicate the direction of energy transportation.

IV. SIMULATION RESULTS

In order to illustrate how a PC composite affects self-collimation, we used a FDTD method to simulate the electromagnetic wave propagation phenomena within two single PC structures (PC_1 and PC_2) and a PC composite (PC_1+PC_2). The FDTD method provides the time-domain solutions of Maxwell's equations by computing the electromagnetic energy in discrete computational grids as functions of time.[34] Our simulation domain consisted of a rectangular area ($60d\times40d$ normalized units, where d is the distance between layers) filled with air and GaN cylinders distributed periodically with a lattice constant a. The simulation domain was discretized into 20 grids per d. Other parameters used in the FDTD simulations were the same as those in the PWE calculations (Sec. II). The entire structure was surrounded by Berenger's perfectly matching layers at the boundaries to avoid reflections in the simulation domain.[35] A narrow-band Gaussian source of TM polarization (E_x, E_y, and H_z) was

Downloaded 14 Mar 2011 to 130.203.246.87. Redistribution subject to AIP license or copyright; see http://jap.aip.org/about/rights_and_permissions

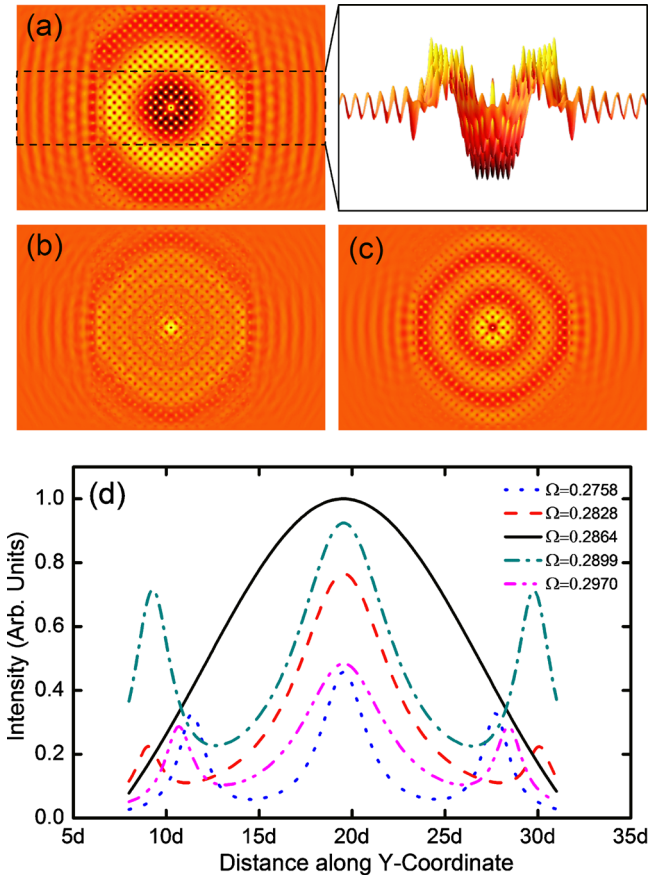

FIG. 4. (Color online) Simulated electromagnetic wave propagation of the PC_1 (31 layer thick in x-coordinate) at a normalized frequency of (a) $\Omega=\omega a/2\pi c=0.2864$, (b) $\Omega=0.2758$, and (c) $\Omega=0.2970$. (d) Wave intensity along y-coordinate measured by the line receiver.

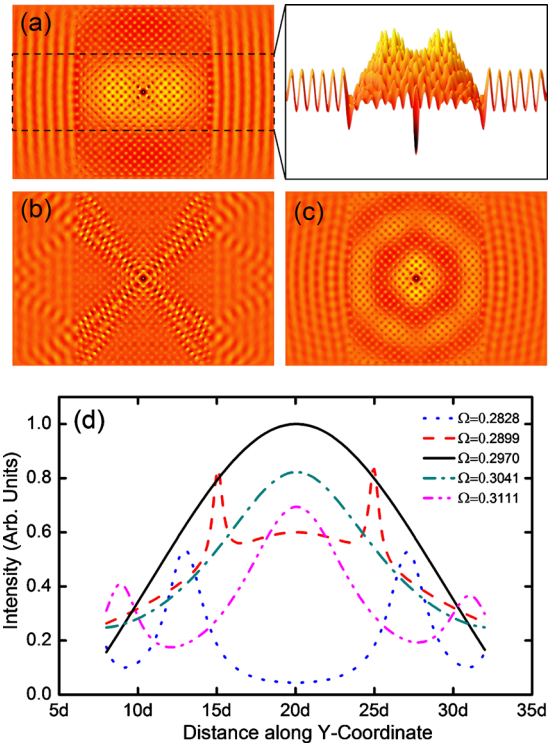

FIG. 5. (Color online) Simulated electromagnetic wave propagation of the PC_2 (31 layers thick in the x-coordinate) at a normalized frequency of (a) $\Omega=0.2970$, (b) $\Omega=0.2828$, and (c) $\Omega=0.3111$. (d) Wave intensity along y-coordinate measured by the line receiver.

placed at the center of the simulation domain and the propagation of electromagnetic energy was monitored. To implement the FDTD method, we used the MEEP FDTD package, which features sub-pixel smoothing for increased accuracy.[36,37] Computations were performed on a high-performance computer that had quad-core 2.6 GHz AMD Opteron processors and 32 GB of ECC RAM.

Two working bands, $\Delta\Omega_1$ ($\Omega=0.2758-0.2970$) and $\Delta\Omega_2$ ($\Omega=0.2828-0.3111$), were chosen to simulate the single PC_1 (maximum self-collimation point $\Omega_{m1}=0.2864$) and PC_2 ($\Omega_{m2}=0.2970$), respectively. A larger band $\Delta\Omega_{1+2}$ ($\Omega=0.2758-0.3111$) was used for the simulation of the PC composite (PC_1+PC_2). A line receiver of length $24d$ was placed at the right edge of the simulation domain, parallel to the y-coordinate, to measure the electromagnetic wave transmittance. Figure 4 depicts the simulated wave propagation results of PC_1 (31 layers thick in the x-coordinate) for different normalized frequencies. As shown in Fig. 4(a), electromagnetic waves at the maximum self-collimation point ($\Omega_{m1}=0.2864$) were collimated along the ΓM orientation after passing through the PC structure. As the wave fronts were parallel to each other in this case, the receiver sensed only one transmittance peak [black curve in Fig. 4(d)]. However, as the frequency deviated from the maximum self-collimation point, the EFC becomes circular, which indicates worse self-collimation [Figs. 4(b) and 4(c)]. As a result, the receiver sensed multiple transmittance peaks due to its multiple-cross with the cocircular wave fronts [Fig. 4(d)]. The field intensity along the y-coordinate measured by the line receiver at different frequencies [Fig. 4(d)] shows that a small deviation in frequency (less than 2% from Ω_{m1}) from the maximum self-collimation point greatly reduced the collimation, as predicted in Sec. III.

The simulated wave propagation results of the 31 layer thick, single PC_2 structure (Fig. 5) are similar to those of PC_1. Electromagnetic waves at the maximum self-collimation point ($\Omega_{m2}=0.2970$) were well-collimated along the ΓM orientation [Fig. 5(a)]. However, once the frequency deviated from the maximum self-collimation point (less than 2.5% from Ω_{m2}), the result of collimation was greatly reduced [Figs. 5(b)–5(d)]. Since the effective refractive index of the PC structure is dependent on the filling fraction and arrangement of the inclusions in the background material,[7] the transmittance of PC_1 is smaller than that of PC_2, as PC_1 has a larger filling ratio and a thus larger effective refractive index.

Based on Figs. 4 and 5, the collimation effect of a single PC structure is limited to a small range (the frequency must be within ±2.5% of the maximum self-collimation point). We expected that a wider collimation range could be achieved by a PC composite structure. The simulated electromagnetic wave propagation results of a PC composite (PC_1+PC_2; PC_1 has 17 layers in the center and PC_2 has 7 layers at each side) are shown in Fig. 6. The simulated results exhibit excellent collimation for a large frequency range ($\Omega=0.2758-0.3111$).

Downloaded 14 Mar 2011 to 130.203.246.87. Redistribution subject to AIP license or copyright; see http://jap.aip.org/about/rights_and_permissions

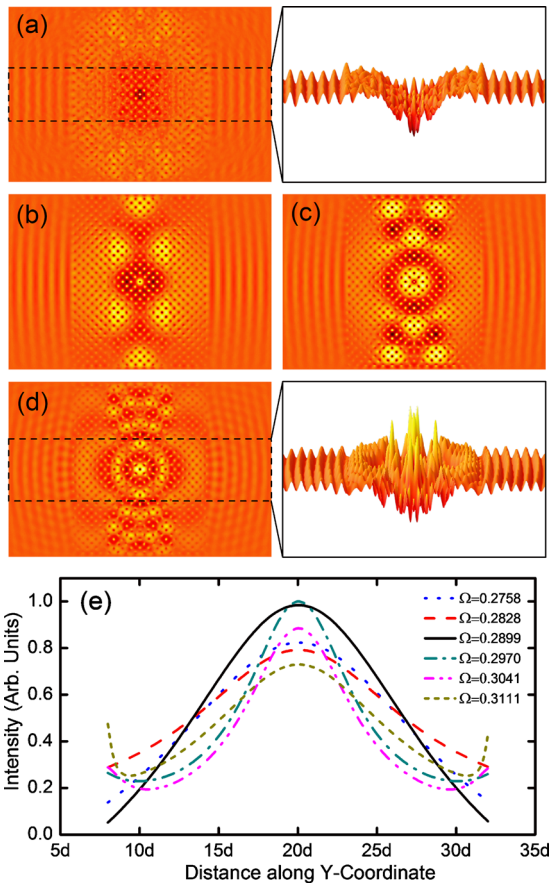

FIG. 6. (Color online) Simulated electromagnetic wave propagation of the PC composite (PC_1+PC_2, PC_1 has 17 layers in the center and PC_2 has 7 layers at each side) at a normalized frequency of (a) $\Omega=0.2758$, (b) $\Omega=0.2899$, (c) $\Omega=0.2970$, and (d) $\Omega=0.3111$. (e) Wave intensity along y-coordinate measured by the line receiver.

Quantitative analysis [Fig. 6(e)] based on the FDTD simulated results indicated that for all the frequencies within $\Delta\Omega_{1+2}$, most waves were collimated and confined in the center region after they passed through the PC composite. The transmittance of the PC composite is between that of PC_1 and PC_2 because the introduction of PC_2 between PC_1 and the background medium serves as a refractive index matching layer, thus improving the transmittance. As a result, the transmittance in the PC composite was comparable to the single PC-based collimation lens, which coincides with the observations in Figs. 4–6. The curvature of the wave fronts after passing through the PC composite are of the same order as those that pass through the single PCs, indicating that the collimation quality is maintained while the working frequency range is broadened. The FDTD-simulated results (Fig. 4–6) indicate that in comparison to single PC structures, a PC composite features better collimation performance in a wider frequency region; this finding was confirmed by the PWE method (Sec. III).

V. SUMMARY

The collimation phenomena of PC composites were investigated numerically through both PWE and FDTD methods. The flat bands were the key to determine the self-collimation characteristics of electromagnetic waves. An optical collimation lens composed of two PCs (GaN cylinders in air) with different filling fractions greatly enlarged the collimation region over a wide frequency range, thereby realizing wide-band optical collimation. The methodology described in this work allows one to confine optical energy flow over long distances of operation, enabling applications such as light-emitting diodes, imaging devices, biosensors, and waveguides.[38–45]

ACKNOWLEDGMENTS

We thank Thomas R. Walker and Michael I. Lapsley for helpful discussions and we acknowledge support from the High Performance Computing Group at the Pennsylvania State University. This work was supported by Air Force Office of Scientific Research (FA9550–08–1–0349), National Science Foundation (ECCS-0824183 and ECCS-0801922), U.S. Department of Agriculture (USDA/NRI), and the Penn State Center for Nanoscale Science (MRSEC).

[1] E. Yablonovitch, Phys. Rev. Lett. **58**, 2059 (1987).
[2] S. John, Phys. Rev. Lett. **58**, 2486 (1987).
[3] K. Ho, C. Chan, and C. Soukoulis, Phys. Rev. Lett. **65**, 3152 (1990).
[4] E. Özbay, A. Abeyta, G. Tuttle, and M. Tringides, Phys. Rev. B **50**, 1945 (1994).
[5] C. Luo, S. G. Johnson, J. D. Joannopoulos, and J. B. Pendry, Phys. Rev. B **65**, 201104(R) (2002).
[6] Z. Feng, X. Zhang, K. Ren, S. Feng, Z. Y. Li, B. Cheng, and D. Zhang, Phys. Rev. B **73**, 075118 (2006).
[7] X. Ao and S. He, Opt. Lett. **30**, 2152 (2005).
[8] M. Mojahedi, E. Schamiloglu, F. Hegeler, and K. J. Malloy, Phys. Rev. E **62**, 5758 (2000).
[9] H. Kosaka, T. Kawashima, A. Tomita, M. Notomi, T. Tamamura, T. Sato, and S. Kawakami, Appl. Phys. Lett. **74**, 1212 (1999).
[10] D. Chigrin, S. Enoch, C. S. Torres, and G. Tayeb, Opt. Express **11**, 1203 (2003).
[11] D. Tang, L. Chen, and W. Ding, Appl. Phys. Lett. **89**, 131120 (2006).
[12] P. T. Rakich, M. S. Dahlem, S. Tandon, M. Ibanescu, M. Soljai, G. S. Petrich, G. D. Joannopoulos, L. A. Kolodziejski, and E. P. Ippen, Nature Mater. **5**, 93 (2006).
[13] S. S. Oh, S. Lee, J. Kim, and H. Y. Park, Opt. Express **15**, 1205 (2007).
[14] A. Matthews, S. K. Morrison, and Y. S. Kivshar, Opt. Commun. **279**, 313 (2007).
[15] Y. Xu, X. J. Chen, S. Lan, Q. Guo, W. Hu, L. J. Wu, and J. Opt, Pure Appl. Opt. **10**, 085201 (2008).
[16] J. Shi, S.-C. S. Lin, and T. J. Huang, Appl. Phys. Lett. **92**, 111901 (2008).
[17] F. Chollet, C. H. Low, S. K. Lee, and C. Yang, Int. J. Comput. Eng. Sci. **4**, 443 (2003).
[18] J. Li, L. Xue, Z. Wang, and Y. Han, Colloid Polym. Sci. **285**, 1037 (2007).
[19] J. S. Skibina, R. Iliew, J. Bethge, M. Bock, D. Fischer, V. I. Beloglasov, R. Wedell, and G. Steinmeyer, Nat. Photonics **2**, 679 (2008).
[20] E. Akmansoy, E. Centeno, K. Vynck, D. Cassagne, and J.-M. Lourtioz, Appl. Phys. Lett. **92**, 133501 (2008).
[21] Q. Wu, J. M. Gibbons, and W. Park, Opt. Express **16**, 16941 (2008).
[22] S.-C. S. Lin, T. J. Huang, J.-H. Sun, and T.-T. Wu, Phys. Rev. B **79**, 094302 (2009).
[23] S.-C. S. Lin and T. J. Huang, J. Appl. Phys. **106**, 053529 (2009).
[24] S.-C. S. Lin, B. R. Tittmann, J.-H. Sun, T.-T. Wu, and T. J. Huang, J. Phys. D: Appl. Phys. **42**, 185502 (2009).
[25] B. K. Juluri, S.-C. S. Lin, T. T. Walker, L. Jensen, and T. J. Huang, Opt. Express **17**, 2997 (2009).
[26] K. M. Leung and Y. Qiu, Phys. Rev. B **48**, 7767 (1993).
[27] L. M. Li and Z. Q. Zhang, Phys. Rev. B **58**, 9587 (1998).
[28] M. Boroditsky, T. F. Krauss, R. Coccioli, R. Vrijen, R. Bhat, and E. Yablonovitch, Appl. Phys. Lett. **75**, 1036 (1999).
[29] S. Satpathy, Z. Zhang, and M. R. Salehpour, Phys. Rev. Lett. **64**, 1239 (1990).
[30] J. D. Joannopoulos, R. D. Meade, and J. N. Winn, *Photonic Crystals: Molding the Flow of Light* (Princeton University Press, Princeton, NJ, 1995).

Downloaded 14 Mar 2011 to 130.203.246.87. Redistribution subject to AIP license or copyright; see http://jap.aip.org/about/rights_and_permissions

[31]T. T. Wu, Z.-G. Huang, and S. Lin, Phys. Rev. B **69**, 094301 (2004).
[32]V. Karathanos, A. Modinos, and N. Stefanou, J. Phys.: Condens. Matter **6**, 6257 (1994).
[33]N. Stefanou, V. Yannopapas, and A. Modinos, Comput. Phys. Commun. **113**, 49 (1998).
[34]A. Taflove and S. C. Hagness, *Computational Electrodynamics: The Finite-Difference Time-Domain Method* (Artech, Norwood, MA, 2000).
[35]J. P. Berenger, J. Comput. Phys. **114**, 185 (1994).
[36]D. Roundy, M. Ibanescu, P. Bermel, A. Farjadpour, J. D. Joannopoulos, and S. G. Johnson, (http://ab-initio.mit.edu/meep/)
[37]A. Farjadpour, D. Roundy, A. Rodriguez, M. Ibanescu, P. Bermel, J. D. Joannopoulos, S. G. Johnson, and G. W. Burr, Opt. Lett. **31**, 2972 (2006).
[38]T. J. Huang, M. Liu, L. D. Knight, W. W. Grody, J. F. Miller, and C.-M. Ho, Nucleic Acids Res. **30**, e55 (2002).
[39]V. K. S. Hsiao, J. R. Waldeisen, Y. Zheng, P. F. Lloyd, T. J. Bunning, and T. J. Huang, J. Mater. Chem. **17**, 4896 (2007).
[40]Y. B. Zheng, T. J. Huang, A. Y. Desai, S. J. Wang, L. K. Tan, H. Gao, and A. C. H. Huan, Appl. Phys. Lett. **90**, 183117 (2007).
[41]Y. B. Zheng, B. K. Juluri, X. Mao, T. R. Walker, and T. J. Huang, J. Appl. Phys. **103**, 014308 (2008).
[42]X. Mao, S.-C. S. Lin, M. I. Lapsley, J. Shi, B. K. Juluri, and T. J. Huang, Lab Chip **9**, 2050 (2009).
[43]M. I. Lapsley, S.-C. S. Lin, X. Mao, and T. J. Huang, Appl. Phys. Lett. **95**, 083507 (2009).
[44]X. Mao, S.-C. S. Lin, C. Dong, and T. J. Huang, Lab Chip **9**, 1583 (2009).
[45]Y. J. Liu, H. T. Dai, X. W. Sun, and T. J. Huang, Opt. Express **17**, 12418 (2009).

Downloaded 14 Mar 2011 to 130.203.246.87. Redistribution subject to AIP license or copyright; see http://jap.aip.org/about/rights_and_permissions